ACS OMEGA

Open Access

http://pubs.acs.org/journal/acsodf

Article

Experimental Study of Transition Metal-Doped Cu-Based Oxygen Carrier for Chemical Looping with Oxygen Uncoupling

Minjun Wang,* Yiming Xu, Ming Xia, Bixiao Zhang, and Yidan Wei

Cite This: *ACS Omega* 2025, 10, 10308−10316

Read Online

ACCESS | Metrics & More | Article Recommendations

ABSTRACT: The Cu-based oxygen carrier exhibits promising potential in the chemical looping with oxygen uncoupling (CLOU) process, wherein its performance is significantly influenced by the characteristics of oxygen release and cyclic reaction stability. In this work, a series of Cu-based oxygen carriers doped with transition metals (Ti, Y, Zr, and Ce) were synthesized by using the sol−gel combustion method and impregnation method. The microstructure, phase structure, O_2 desorption, and cyclic reaction of Cu-based oxygen carriers were studied by experiments. The results show that (1) the doped element loading rate, specific surface area, average pore size, and pore volume of the oxygen carrier prepared by the sol−gel combustion method surpass those achieved through the impregnation method; (2) Ce doping formed a solid solution with CuO and $CuAl_2O_4$ without altering the main crystal phases, while Zr, Ti, and Y doping resulted in the formation of distinct phases; (3) the doped samples exhibit superior oxygen release performance compared to the undoped ones, with Ce-doped carriers demonstrating the highest level of performance; and (4) the cycling stability of Cu-based oxygen carriers is significantly enhanced by Ce doping. The aforementioned results collectively demonstrate the remarkable efficacy of Ce doping as a highly effective modification technique for Cu-based oxygen carriers. Furthermore, the sol−gel combustion method emerges as a superior method for preparing doped oxygen carriers.

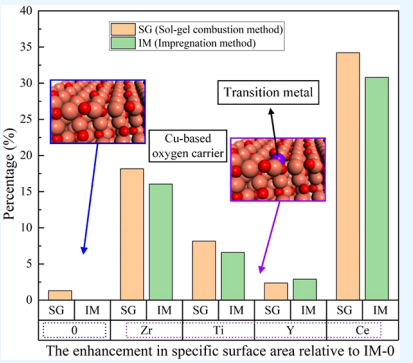

1. INTRODUCTION

The greenhouse effect, primarily driven by the dominance of CO_2 as a greenhouse gas, has emerged as a pressing global environmental concern.[1] The combustion of fossil fuels stands out as the primary catalyst behind the substantial increase in atmospheric CO_2 levels. Chemical looping combustion (CLC) represents a groundbreaking combustion technique amidst many CO_2 emission reduction technologies. The fundamental principle of CLC involves breaking down the coal combustion reaction into two distinct steps, which are conducted in separate fuel and air reactors, respectively. By facilitating the continuous circulation of oxygen carriers, this process enables the provision of oxygen from the air to the fuel, thereby accomplishing complete fuel combustion. The CLC process is illustrated in Figure 1, and the simplified reaction equations for the two-step reaction are presented below.

$$\text{Fuel} + MeO_x \rightarrow CO_2 + H_2O + MeO_{x-1} \quad (1)$$

$$2MeO_{x-1} + O_2 \rightarrow 2MeO_x \quad (2)$$

The CLC process exhibits zero energy separation of CO_2, thereby enhancing the thermal efficiency of the system and effectively suppressing the formation of other pollutants, such as dioxins. These advantages offer significant economic benefits. However, it has been observed that there is no direct solid-state reaction between the oxygen carrier and solid fuel, such as coal; instead, the predominant interaction occurs through a gas−solid reaction between the products of coal gasification and the oxygen carrier. The disparity in rates between coal gasification and the reaction rate of the oxygen carrier/coal gasification product hinders complete coal conversion, thereby posing significant challenges for CO_2 capture.

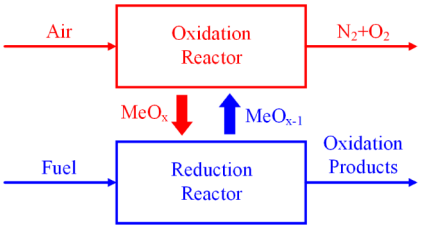

Figure 1. Schematic diagram of the CLC process.

Received: November 2, 2024
Revised: February 12, 2025
Accepted: February 26, 2025
Published: March 7, 2025

To address the aforementioned issues, Mattisson et al. proposed a technique known as chemical looping with oxygen uncoupling (CLOU).[2,3] The CLOU employs metal oxides, including Cu-based oxide,[4−7] Mn-based oxide,[8−10] and perovskite,[11−13] as oxygen carriers capable of releasing O_2 at lower temperatures and under reduced partial pressure of oxygen. The reaction steps are specifically illustrated in eqs 3, 4, and 5. The overall reaction of CLOU exhibits similarities to the CLC process employed with coal; however, a distinguishing factor lies in the direct combustion of coal within an O_2 atmosphere in CLOU, thereby eliminating the rate-limiting step associated with coal gasification. The Cu-based oxygen carrier is regarded as a favorable choice for CLOU due to its high capacity for carrying oxygen and its cost-effectiveness. The study conducted by Mattisson et al.[3] revealed that the reaction rate of the Cu-based oxygen carrier with petroleum coke in the CLOU process was approximately 50 times higher compared to the Fe-based oxygen carrier in the CLC process.

$$2MeO_x \rightarrow O_2 + 2MeO_{x-1} \quad (3)$$

$$Fuel + O_2 \rightarrow CO_2 + H_2O \quad (4)$$

$$O_2 + 2MeO_{x-1} \rightarrow 2MeO_x \quad (5)$$

Although the utilization of CLOU with CuO as an oxygen carrier can effectively enhance the coal reaction rate, its major drawback lies in the low melting point and susceptibility to sintering of the Cu-based oxygen carrier. Additionally, the lattice oxygen in the resulting Cu_2O product is not fully utilized after oxygen release, leading to increased transfer rates and storage of the oxygen carrier within the fuel reactor during complete coal conversion. Therefore, it is imperative to investigate modifications for the enhancement of Cu-based oxygen carriers.

The loading of the active component onto the inert component represents one of the most extensively employed strategies for enhancing the stability of oxygen carriers. Currently, the predominant inert carriers employed include Al_2O_3,[14−16] SiO_2,[14,17,18] ZrO_2,[19,20] TiO_2,[21] MgO,[22] YSZ (yttrium-stabilized zirconia),[23] bentonite,[24] and sepiolite.[25] Although the incorporation of an inert carrier can enhance the resistance of the oxygen carrier against sintering, agglomeration, and wear, it also results in a relative reduction in the active ingredient content, thereby decreasing the oxygen capacity per unit mass and increasing system volume and oxygen carrier usage. Another approach to modify the oxygen carrier system involves incorporating active additives based on alkali or alkaline earth metals during its preparation.[26−30] Imtiaz et al.[26] discovered that the presence of K^+ ions can increase the concentration of CuO, which is the active component in Cu-based oxygen carriers. Bao et al.[27] demonstrated that the introduction of K^+ ions significantly enhances the porosity and specific surface area of oxygen carriers. Nevertheless, it is noteworthy that alkali metals and their compounds are also emitted as detrimental pollutants during the coal combustion process, thereby accelerating the accumulation of ash and slag on the heating surface.[31] The low melting points of alkali metals and alkaline earth metals can also induce sintering or agglomeration of oxygen carrier particles. It is imperative to identify more appropriate doping modification constituents.

Several studies have demonstrated that the incorporation of transition metal elements can significantly enhance the properties associated with hydrogen and oxygen storage materials, such as improving the kinetics of gas molecule release and absorption (such as H_2 and O_2), increasing material capacity, and enhancing material cycle stability. The presence of Ti can induce distortion in the oxygen lattice within the material, leading to a synergistic effect of catalysis and nanospace confinement. This consequently enhances material reactivity and reduces reaction temperature, which is highly advantageous for preventing oxygen carrier sintering.[32,33] The incorporation of Y can enhance the oxygen vacancy concentration and oxygen storage capacity of relevant oxygen storage materials, while simultaneously improving their thermal stability.[34,35] The addition of Zr can enhance the reactivity and oxygen storage capacity of oxygen carriers, materials for oxygen storage, and catalysts.[36−38] Ce-doped Fe-based oxygen carriers were prepared by Galvita et al.[39] using the coprecipitation method, and experimental results demonstrated enhanced reactivity and stability compared to single Fe-based oxygen carriers.

The aforementioned research findings hold significant implications for enhancing the reactivity, oxygen-carrying capacity, and stability of Cu-based oxygen carriers. In this work, a series of Cu-based oxygen carriers doped with transition metals (Ti, Y, Zr, and Ce) were synthesized using the sol−gel combustion method and impregnation method. The doped oxygen carriers were designated as Me_{tr}-CuO. The microstructure, phase structure, surface topography, oxygen decoupling performance, content of doped elements, and cyclic reactivity of Me_{tr}-CuO were studied. The objective of this work is to investigate the impact of various transition metal doping on Cu-based oxygen carriers and explore the influence of different preparation methods on the performance of doped oxygen carriers. The findings of this study will provide valuable insights for the design and development of oxygen carriers in CLOU.

2. EXPERIMENTAL METHODS

2.1. Oxygen Carriers Synthesis. In this study, two preparation methods were employed to synthesize transition metal-doped Cu-based oxygen carriers, namely the sol−gel combustion method and the impregnation method. $CuAl_2O_4$ was utilized as an inert support material with a mass fraction of 60 wt % for CuO. The doping levels of transition metal were 5 wt % with respect to $CuO/CuAl_2O_4$. The initial reagents include $Cu(NO_3)_2{\cdot}3H_2O$, $Al(NO_3)_3{\cdot}9H_2O$, $C_{16}H_{36}O_4Ti$, $Y(NO_3)_3{\cdot}6H_2O$, $Zr(NO_3)_4{\cdot}5H_2O$, $Ce(NO_3)_3{\cdot}6H_2O$, citric acid ($C_6H_8O_7{\cdot}H_2O$), and deionized water.

2.1.1. Sol−Gel Combustion Method. The stoichiometric amounts of the metallic compound and citric acid were initially dissolved in deionized water to generate a homogeneous solution. Then, the solution was placed on a constant-temperature magnetic stirrer and stirred at a consistent speed, while the water bath temperature was set to 75 °C. The mixture was left undisturbed until it formed a thick gel in the beaker. Subsequently, the gel obtained from the previous step was transferred to a drying oven for 12 h at 90 °C. Following this, the dried gel was introduced into a muffle furnace preheated to 650 °C and removed once it burned to form black particles. Next, the muffle furnace was heated up to 850 °C, and the black particles obtained earlier were subjected to high-temperature calcination for 6 h. Finally, the oxygen carrier particles were acquired by grinding and calcining the resulting powder.

https://doi.org/10.1021/acsomega.4c09980
ACS Omega 2025, 10, 10308−10316

2.1.2. Impregnation Method. The stoichiometric amounts of the metallic compound and $CuO/CuAl_2O_4$ were initially dissolved in deionized water. The resulting mixture was thoroughly stirred and placed in a drying oven, where it was dried at 90 °C for 12 h. Subsequently, the dried sample was subjected to calcination at 650 °C for 6 h using a muffle furnace. Following the cooling process, oxygen carrier particles were obtained through grinding. The oxygen carriers were denoted as SG-*Mx* and IM-*Mx*, corresponding to the sol−gel combustion method (SG) and impregnation method (IM), respectively. Here, *M* represents the doped element, while *x* denotes the mass fraction (%) of the doped component.

2.2. Sample Characterization and Thermogravimetric Experiment. The X-ray diffraction (XRD) analysis was performed using the Panalytical, The Netherlands' X'Pert PRO X-ray diffractometer. Cu−Kα radiation (λ = 0.154 Å) with a step width of 0.02° was utilized, while an operating voltage and tube current of 40 kV and 40 mA, respectively, were employed for data collection through a timed step scanning method within a scanning range of 10 to 90°. The specific surface area analysis was conducted using the ASAP2010 specific surface area and pore size analyzer manufactured by Micromeritics. The liquid nitrogen saturation temperature was set at 77 K, with an aperture measurement range of 1.7 to 300 nm. The relative pressure (P/P_0) ranged from 0.01 to 0.995 (where P and P_0 represent the low-temperature adsorption equilibrium pressure and saturation pressure of liquid nitrogen, respectively). Prior to measurement, the test sample underwent a vacuum treatment at a temperature of 105 °C to eliminate impurity gases. The specific surface area of the sample was determined using the Brunauer-Emmett-Teller (BET) equation, while the pore volume was calculated employing the T-curve method. Additionally, the pore size distribution was assessed by utilizing the Barrett−Joyner−Halenda (BJH) model. The Elan DRC-e inductively coupled plasma mass spectrometer (ICP-MS, PerkinElmer, USA) was employed for the determination of the transition metal content in the oxygen carrier.

The STA409 (Netzsch, Germany) thermogravimetric analyzer (TGA) was employed to conduct the programmed temperature reaction of the oxygen carrier oxygen release reaction, enabling preliminary determination of the performance and reaction rate of the oxygen release process. A specific amount of oxygen carrier was weighed into the crucible, followed by injection of pure N_2 at a flow rate of 50 mL/min. Simultaneously, it was heated to 1000 °C at a heating rate of 10 °C/min until the sample reached complete reaction, indicated by no change in mass. Subsequently, the N_2 flow was then maintained until the reactor temperature reached ambient conditions.

3. RESULTS AND DISCUSSION

3.1. BET Surface. In order to investigate the impact of four transition metal elements on the microstructure of Cu-based oxygen carrier particles, BET analysis was employed to examine Me_{tr}-CuO prepared by using different methods. The experimental results for the specific surface area, average pore size, and pore volume of each sample are presented in Table 1.

The specific surface areas of undoped, Zr-doped, Ti-doped, and Ce-doped Cu-based oxygen carriers prepared by the sol−gel combustion method are found to be 3.85, 4.49, 4.11, and 5.10 m^2/g, respectively. In comparison, the specific surface areas of Cu-based oxygen carriers prepared by the impregnation method were measured as 3.80, 4.41, 4.05, and 4.97 m^2/g, respectively. Notably, the sol−gel combustion method yielded a significantly higher specific surface area for the Cu-based oxygen carrier. Simultaneously, the oxygen carrier prepared by the sol−gel combustion method exhibits higher average pore size and pore volume compared to that prepared by the impregnation method. The average pore size and pore volume of the Ce-doped Cu-based oxygen carrier, prepared using the sol−gel combustion method, are 2.06% and 9.68% higher than those obtained through the impregnation method, respectively. The largest difference between the two preparation methods lies in the average pore size of Cu-based oxygen carriers without transition element doping, which reaches a significant increase of 12.3%. The observed phenomenon can be attributed to the addition of a substantial amount of citric acid as a complexing and gelling agent during the sol−gel combustion method preparation process, resulting in the formation of citric acid complexes with Cu, Al, and transition metal ions as precursors. Upon high-temperature combustion, these citric acid complexes decompose, generating numerous gases and pores. Consequently, this leads to an increase in the specific surface area, average pore size, and pore volume of the oxygen carrier. Conversely, in the impregnation method, the presence of hydrated OH^- on the surface of the precursor during drying and calcination facilitates hydrogen bonding, leading to particle agglomeration and a subsequent reduction in the specific surface area, average pore size, and pore volume of the sample.

Table 1. BET Data for the Fresh Cu-Based Oxygen Carriers

oxygen carrier	specific surface area (m^2/g)	average pore size (nm)	pore volume (cm^3/g)
SG-0	3.85	12.8	0.015
IM-0	3.80	11.4	0.013
SG-Zr5	4.49	26.1	0.028
IM-Zr5	4.41	25.9	0.024
SG-Ti5	4.11	22.7	0.020
IM -Ti5	4.05	22.0	0.019
SG-Y5	3.89	18.5	0.018
IM -Y5	3.91	19.2	0.021
SG-Ce5	5.10	24.3	0.031
IM -Ce5	4.97	23.8	0.028

In contrast to the aforementioned four, the sol−gel combustion method yielded a *Y*-doped Cu-based oxygen carrier with a specific surface area of 3.89 m^2/g, an average pore size of 18.5 nm, and a pore size of 0.018 cm^3/g. These values are slightly lower than those obtained through the impregnation method (specific surface area: 3.91 m^2/g; average pore size: 19.2 nm; pore volume: 0.021 cm^3/g). The difficulty in forming a complex between the Y element and citric acid in the precursor mixture may account for this phenomenon, as it also hinders the formation of complexes between Cu and Al ions with citric acid. Consequently, this impedes pore formation during combustion and calcination, resulting in a reduction in specific surface area, average pore size, and pore volume of the sample.

On the other hand, the BET results demonstrate a significant increase in the specific surface area of the doped oxygen carrier compared to the undoped Cu-based oxygen carrier. The enhancement in the specific surface area of the oxygen carriers relative to IM-0 is illustrated in Figure 2. The

https://doi.org/10.1021/acsomega.4c09980
ACS Omega 2025, 10, 10308−10316

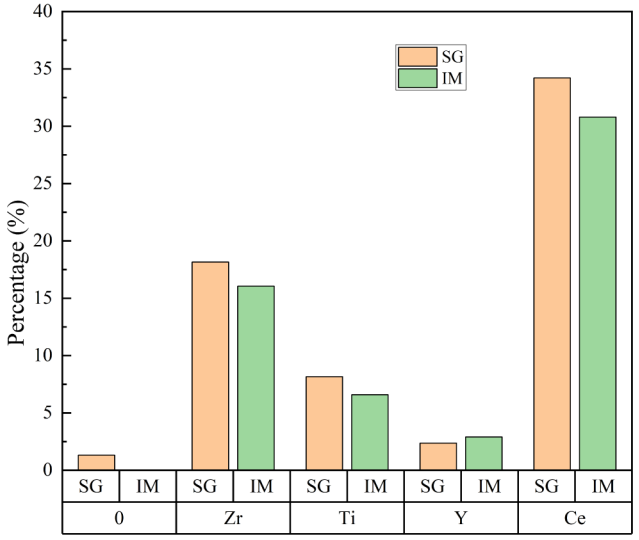

Figure 2. Enhancement in specific surface area of the oxygen carriers relative to IM-0.

specific surface area of the sample prepared by the sol−gel combustion method is 3.85 m^2/g without doping, whereas after Zr, Ti, Y, and Ce doping, the specific surface area increases to 4.49, 4.11, 3.89, and 5.10 m^2/g respectively, representing enhancements of 18.2%, 8.2%, 2.4%, and 34.2%. These findings demonstrate that transition element doping effectively enhances the specific surface area of Cu-based oxygen carriers, thereby augmenting the chemical reaction area and improving reactivity in CLOU. The effects of four types of transition metal doping on the specific surface area, average pore size, and pore volume of oxygen carriers follow the order: Ce > Zr > Ti > Y. Notably, the sol−gel combustion method for preparing Ce-doped oxygen carriers yields significant enhancements in specific surface area (5.10 m^2/g), average pore size (24.3 nm), and pore volume (0.031 cm^3/g). These values increase by as much as 32.4%, 89.8%, and 106.6% compared to undoped oxygen carriers, respectively. Conversely, the enhancement of specific surface area, average pore size, and pore volume in Y-doped copper-based oxygen carriers is marginal, potentially attributed to the limited formation of complexes during precursor synthesis.

3.2. XRD Analysis. The crystal phase structure of transition metal-doped Cu-based oxygen carriers, obtained through various preparation methods, was characterized by using XRD. The corresponding results are presented in Figures 3 and 4.

The XRD patterns of the oxygen carriers prepared by both methods exhibit sharp peaks, indicating a relatively complete crystallization process. The XRD profiles of carriers prepared without transition metals reveal the presence of only the expected main crystal phases, CuO and $CuAl_2O_4$. It can be observed from the XRD patterns that the diffraction peak of the Ce-doped oxygen carrier prepared by both methods exhibits a leftward shift. This shift occurs because the ionic radius of the Ce ion (0.097 nm) is larger than that of the Cu ion (0.073 nm). Consequently, the incorporation of Ce into the copper oxide lattice induces lattice expansion.

The XRD patterns of oxygen carrier samples incorporating 5% Zr, Ti, and Y elements revealed a minor peak. By comparing with reference spectra, it can be deduced that these composite peaks are attributed to the presence of cubic-phase

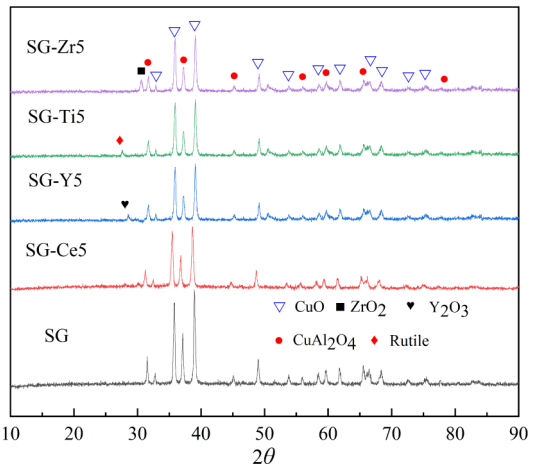

Figure 3. XRD patterns of Me_{tr}-CuO prepared by the sol−gel combustion method.

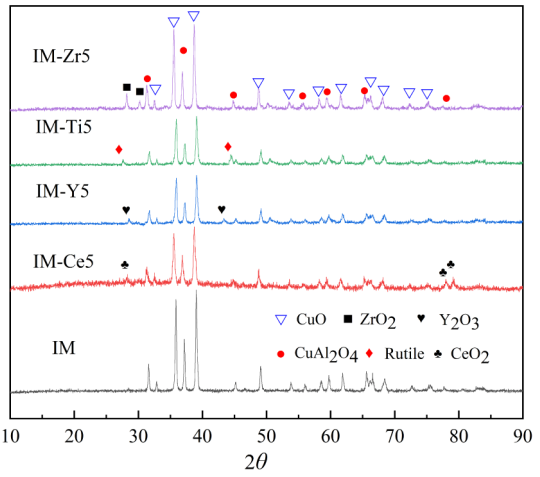

Figure 4. XRD patterns of Me_{tr}-CuO prepared by the impregnation method.

ZrO_2, anatase-phase TiO_2, and Y_2O_3, respectively. This finding implies restricted solid solubility for Zr, Ti, and Y transition metals within $CuO/CuAl_2O_4$. In contrast, the XRD pattern of the sample prepared by the sol−gel combustion method does not exhibit distinct heterogeneous peaks upon the addition of 5% Ce element. This may be attributed to the presence of Ce in a divided state, which is below the detection limit of XRD. The results indicate that CuO and $CuAl_2O_4$ are the predominant crystalline phases of the Cu-based oxygen carrier. Despite the addition of Ce, the crystal structures of CuO and $CuAl_2O_4$ remain unaltered, and Ce successfully incorporates into the primary lattice without forming separate phases. To further investigate the uniformity of Ce-doped Cu-based oxygen carrier, ICP-MS analysis was conducted on five batches of SG-Ce5 samples. The results are listed in Table 2. The results indicate that in five distinct batches of SG-Ce5 samples, the proportions of Ce are measured at 4.93%, 4.91%, 4.91%,

Table 2. Mass Fraction of the SG-Ce5 Samples

batch	1	2	3	4	5
theoretical value (%)	5	5	5	5	5
actual value (%)	4.93	4.91	4.91	4.90	4.95

https://doi.org/10.1021/acsomega.4c09980
ACS Omega 2025, 10, 10308−10316

4.90%, and 4.95%, respectively, yielding an average concentration of 4.92%. This value is closely aligned with the designed ratio of 5%. In conjunction with the preceding XRD analysis, it can be reasonably inferred that the Ce is likely to be doped uniformly.

The XRD pattern of the sample prepared by the impregnation method, with an addition of 5% Ce element, exhibited distinct mixed peaks that were identified as CeO_2. Similarly, the XRD patterns of oxygen carrier samples containing 5% Zr, Ti, and Y elements also displayed mixed peaks. The XRD pattern of samples prepared using the impregnation method demonstrates higher intensity and sharper peak patterns than those obtained through the sol−gel combustion method, suggesting a substantial decrease in the transition metal loading during impregnation. However, while only the Ce-doped Cu-based oxygen carrier prepared using the sol−gel combustion method exhibits no change in crystal structure, other samples display heterogeneous phases. Nevertheless, studies have shown that these heterogeneous phases, such as ZrO_2, TiO_2, and Y_2O_3, can enhance the thermal and mechanical stability of the oxygen carrier. CeO_2 is a major constituent of a cerium−zirconium solid solution, which is commonly employed as an important oxygen storage material and may potentially contribute to increasing the oxygen-carrying capacity of Cu-based oxygen carriers.[40−42]

3.3. TGA Analysis. According to the principle of CLOU, the oxygen release performance of an oxygen carrier plays a pivotal role in its overall functionality. To investigate the oxygen release performance of Cu-based oxygen carriers doped with different transition metals, thermogravimetric experiments were conducted on the transition metal-doped oxygen carriers prepared using two different methods. The experimental results are presented in Figures 5 and 6.

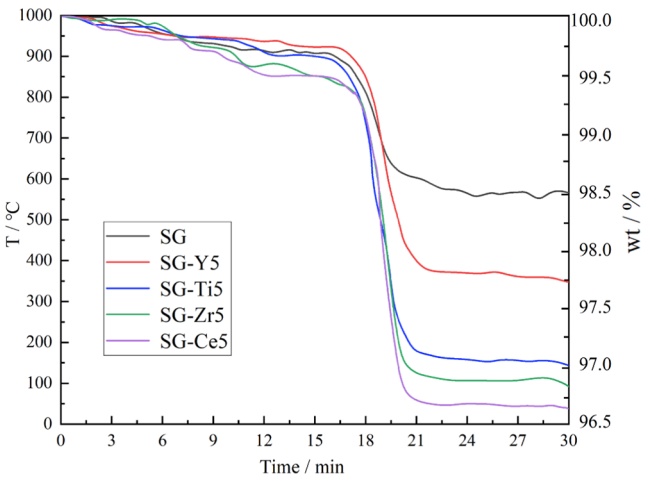

Figure 5. TGA curves of Me_{tr}-CuO prepared by the sol−gel combustion.

The figures illustrate that the prepared Cu-based oxygen carriers exhibit rapid decomposition and oxygen release within the temperature range of 850−910 °C, thereby satisfying the theoretical requirements for chemical chain decoupling combustion. The oxygen release of the transition metal-doped samples is significantly higher than that of the undoped samples, indicating that the addition of transition metals can effectively enhance the oxygen release performance of copper-based oxygen carriers. Moreover, it is observed that the oxygen

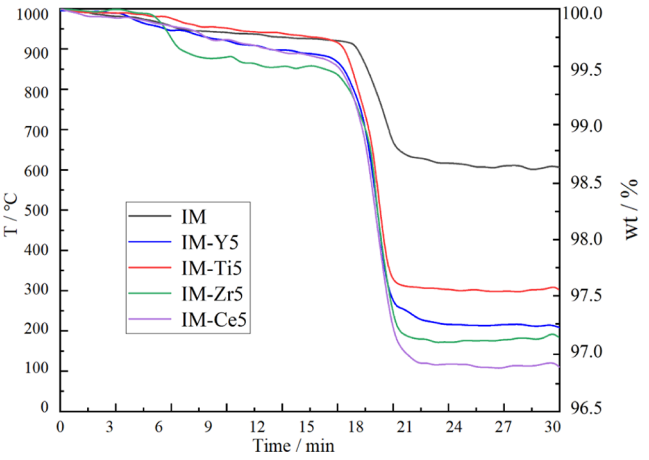

Figure 6. TGA curves of Me_{tr}-CuO prepared by the impregnation method.

release temperature of the doped sample is lower than that of the undoped sample, suggesting enhanced chemical reactivity attributed to transition metal doping. This improvement is further corroborated by the analysis of the average oxygen release rate (Figure 7). The Ce-doped Cu-based oxygen carrier

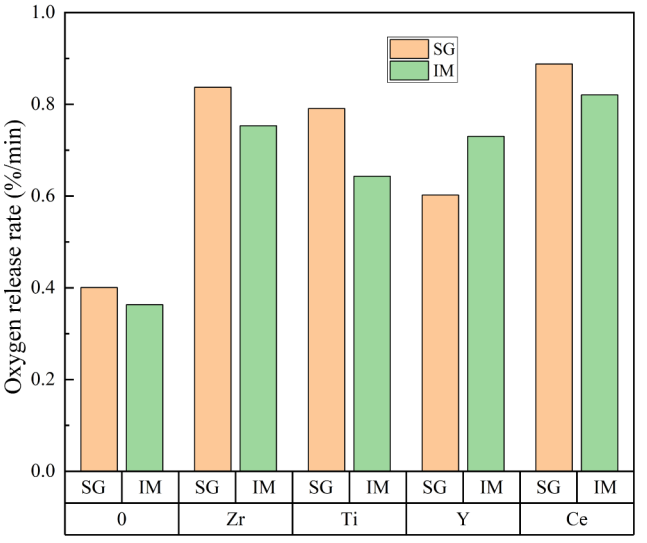

Figure 7. Average oxygen release reaction rate of Me_{tr}-CuO.

exhibits the fastest rate of oxygen release, which can be attributed to the reduction in the migration barrier of oxygen ions within CuO and the decreased formation barrier of oxygen molecules facilitated by Ce. In contrast, the effect of Y-doped Cu-based oxygen carriers on oxygen release and reactivity is less significant, likely due to the relatively low concentration of Y in the samples prepared by both methods.

By further comparison of the two preparation methods, it can be observed that the oxygen release capacity of the carrier prepared using the sol−gel combustion method is marginally higher than that of the sample prepared through impregnation. For instance, after doping with Ce on a Cu-based oxygen carrier, the mass ratio of released oxygen achieved by sol−gel combustion (96.58%) is slightly lower compared to that achieved by impregnation (96.89%), indicating a greater oxygen release capability for samples prepared via sol−gel combustion. This trend holds true for other transition metal-

https://doi.org/10.1021/acsomega.4c09980
ACS Omega 2025, 10, 10308−10316

doped carriers as well. It is noteworthy that when considering carriers doped with transition metals, there exists minimal disparity in their oxygen release performance between both preparation methods, suggesting that variations in loading transition metal elements may account for differences in oxygen release performance.

3.4. Cycle Behavior of the Oxygen Carrier. The oxygen carrier utilized for coal CLOU necessitates excellent long-term, multicycle reactivity. Therefore, an investigation into the cyclic reaction capability of a Cu-based oxygen carrier is imperative. The results obtained from BET, XRD, and TGA experiments on all prepared samples demonstrate that the addition of the Ce element exhibits the most significant impact in enhancing the reactivity of Cu-based oxygen carriers. Consequently, a comprehensive analysis is conducted on the cyclic thermogravimetric experimental outcomes of three samples: the undoped sample, the Ce-doped sample prepared via the sol−gel combustion method, and the Ce-doped sample prepared through the impregnation method. The oxygen release from the three samples during 20 cycles of the reaction process is depicted in Figure 8.

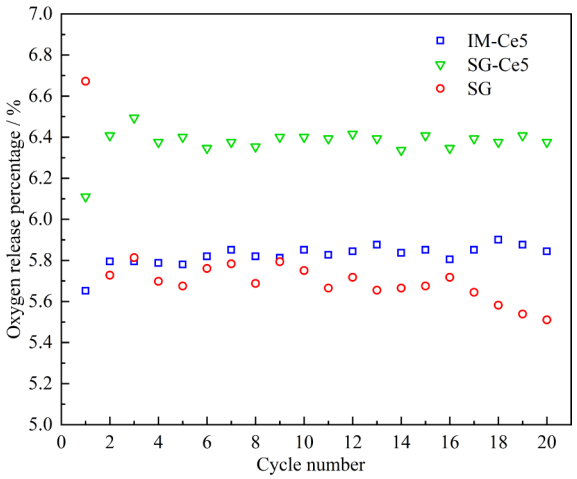

Figure 8. Multiple absorption−desorption cycles of the Cu-based oxygen carriers.

It can be observed that the initial decomposition reaction of the undoped Cu-based oxygen carrier exhibits a remarkably high rate of oxygen evolution, which subsequently diminishes, possibly due to slight sintering occurring on the surface of carrier particles during the oxygen desorption−oxygen absorption reaction. However, in the third cycle reaction, there is a slight increase in oxygen desorption, potentially attributed to pore enlargement within particle interiors induced by thermal shock and chemical reactions. Subsequently, fluctuations are observed in the oxygen desorption process while maintaining overall stable performance. The oxygen release rate of the oxygen carrier continued to decrease until the onset of the 17th cycle, potentially attributed to intensified sintering and agglomeration phenomena resulting from repeated cycling reactions. The oxygen release of the Ce-doped Cu-based oxygen carrier is significantly higher compared to the undoped sample. Meanwhile, notable distinctions exist between the Ce-doped Cu oxygen carriers prepared by using two different methods. In the case of impregnation-method-prepared Ce-doped oxygen carriers, there is no decrease in oxygen release during the second reaction; instead, an increase is observed. Furthermore, after multiple cycles, the oxygen release reaction is similar to that of the undoped samples. Although a decreasing trend in oxygen release is observed for Ce-doped carriers after 16 cycles, it occurs at a relatively slower rate. These findings indicate that doping of Ce enhances the stability of Cu-based oxygen carriers, a result consistent with observations of Ce-doped Fe-based oxygen carriers. Studies have demonstrated that Ce-doped Fe-based oxygen carriers exhibit superior resistance to particle sintering, thereby markedly improving their stability.[39,43,44] It is important to note that the inert support ($CuAl_2O_4$) may have a coeffect with the Ce dopant on the Cu-based oxygen carrier. Further studies will be carried out to examine the interaction between the inert support and the doping element. On the other hand, the oxygen release of the Ce-doped oxygen carrier prepared by the sol−gel combustion method is significantly higher compared to the previous two samples. Furthermore, this sample exhibits an increasing trend in oxygen release during the initial three reactions and demonstrates exceptional stability and high oxygen release throughout subsequent cyclic reactions, without any significant or continuous decline. These findings suggest that the sol−gel combustion method is more suitable for synthesizing Cu-based oxygen carriers with enhanced performance.

3.5. ICP-MS Analysis. The results of the thermogravimetric oxygen release experiment for a Cu-based oxygen carrier suggest that the disparity in oxygen release performance between samples prepared using two different methods may be attributed to variations in the transition metal loading. To validate this hypothesis, ICP-MS analysis was conducted to determine the content of transition metal elements incorporated into the oxygen carrier. Table 3 presents the theoretical value, actual value, and residual value of the transition metal content after 20 cycles. The reduction value of doped element loading after 20 reaction cycles is shown in Figure 9.

Table 3. Mass Fraction of the Transition Metal in Me_{tr}-CuO Prepared by Different Methods

oxygen carriers	theoretical value (%)	actual value (%)	value after 20 cycles (%)
SG-Zr5	5	4.32	4.03
IM-Zr5	5	4.28	4.01
SG-Ti5	5	4.29	4.05
IM -Ti5	5	4.17	3.98
SG-Y5	5	3.92	3.65
IM -Y5	5	3.11	2.99
SG-Ce5	5	4.92	4.77
IM -Ce5	5	4.45	4.16

The actual transition metal contents in Zr, Ti, Y, and Ce-doped oxygen carriers prepared by the sol−gel combustion method are 4.32%, 4.29%, 3.92%, and 4.92%, respectively. These values exceed those obtained from the impregnation method (4.28%, 4.17%, 3.11%, and 4.45%). This observation suggests that the sol−gel combustion method facilitates a more efficient loading of transition metal elements compared with the impregnation method, thereby enhancing their presence on the oxygen carriers. Among these samples, the Ce-doped oxygen carrier exhibits the highest Ce load, which closely approaches its theoretical value, while the Y-doped oxygen carrier demonstrates relatively lower Y content consistent with XRD results.

https://doi.org/10.1021/acsomega.4c09980
ACS Omega 2025, 10, 10308−10316

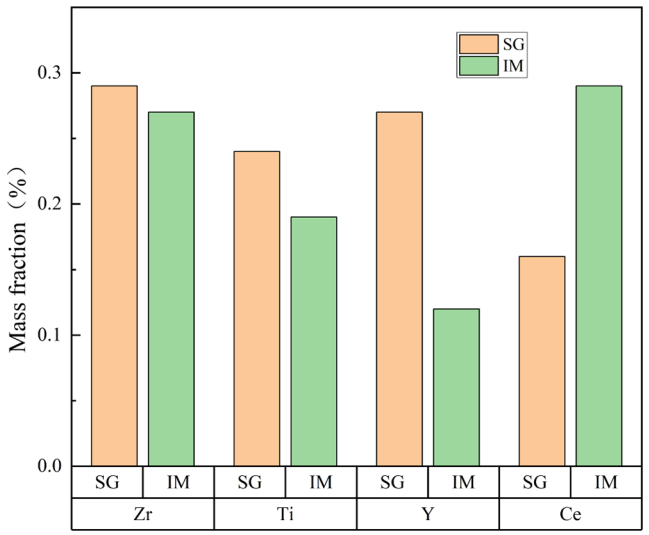

Figure 9. Reduction value of doped element loading after undergoing 20 reaction cycles.

After analyzing the transition metal content in the sample after 20 cycles, it is evident that the observed trend aligns completely with the actual values. The loading sequence still follows Ce5 > Zr5 > Ti5 > Y5 and SG > IM, which effectively explains the oxygen release pattern observed in thermogravimetric experiments (Ce5 > Zr5 > Ti5 > Y5 and SG > IM) and validates our initial hypothesis. Furthermore, it is noteworthy that even after 20 cycles, the Ce loading capacity in the sol−gel combustion-prepared Ce-doped oxygen carrier remains close to its theoretical value at an impressive 4.77%, with only a marginal decrease of 0.15% (see Figure 9). This can be attributed to the complete incorporation of all Ce elements into the main lattice of $CuO/CuAl_2O_4$ within the SG-Ce5 sample. However, a significant decrease in Y loading to 2.99% was observed after 20 cycles, indicating a substantial loss of the Y element. It is worth noting that the optimal doping ratio of Ce in Cu-based oxygen carriers requires further investigation.

4. CONCLUSIONS

The present study successfully synthesized a series of Cu-based oxygen carriers doped with transition metals (Ti, Y, Zr, and Ce) using the sol−gel combustion method and the impregnation method. Subsequently, the impact of these transition metal dopants on the phase structure, oxygen release performance, and cyclic reactivity of Cu-based oxygen carriers was thoroughly investigated. The BET analysis reveals a significant increase in the specific surface area, average pore diameter, and pore volume of Me_{tr}-CuO compared to undoped Cu-based oxygen carriers. Specifically, the specific surface area (5.10 m^2/g), average pore size (24.3 nm), and pore volume (0.031 cm^3/g) of the Ce-doped carrier prepared through the sol−gel combustion method exhibit remarkable improvements. These values are enhanced by 32.4%, 89.8%, and 106.6%, respectively, when compared to undoped oxygen carriers. The XRD patterns of the oxygen carrier prepared by both methods exhibit sharp peaks, indicating a relatively complete crystallization process. Among all of the samples, only in the SG-Ce5 sample does Ce form a solid solution with CuO and $CuAl_2O_4$ without undergoing any noticeable phase transformation, while doping with Zr, Ti, and Y leads to the formation of distinct phases. The results of the TGA experiment demonstrate a decrease in the oxygen release temperature of Me_{tr}-CuO, with higher oxygen release observed for the doped carrier compared to the undoped counterpart. Additionally, the oxygen release pattern follows Ce > Zr > Ti > Y, with SG-*Mx* exhibiting more oxygen release than IM-Mx. The results of the cyclic reaction show that the Ce-doped Cu-based oxygen carrier, prepared via the sol−gel combustion method, exhibits sustained high oxygen release even after undergoing 20 cycles of reaction. This phenomenon can be attributed to the elevated loading rate of the Ce element, as confirmed by ICP-MS analysis. Specifically, ICP-MS analysis reveals a marginal decrease in the load rate of the Ce-SG element from 4.92% to 4.77% after 20 cycles (a reduction of only 0.15%). In contrast, the load rate of Y for sample IM-Y5 is merely 2.99% following the completion of 20 cycles. The aforementioned results collectively demonstrate the remarkable efficacy of Ce doping as an exceptionally effective modification technique for Cu-based oxygen carriers. Moreover, the sol−gel combustion method emerges as a superior approach for preparing doped oxygen carriers. This study would be helpful in rationalizing the development of a high-performance oxygen carrier for CLOU. In future work, we will further investigate the microstructure and reaction mechanism of Ce-doped Cu-based oxygen carriers in CLOU.

AUTHOR INFORMATION

Corresponding Author

Minjun Wang − *School of Energy and Power, Jiangsu University of Science and Technology, Zhenjiang 212003, China*; orcid.org/0009-0005-1863-2780; Email: wmj403@just.edu.cn

Authors

Yiming Xu − *School of Energy and Power, Jiangsu University of Science and Technology, Zhenjiang 212003, China*

Ming Xia − *Chuzhou Cigarette Factory, China Tobacco Anhui Industrial Co., Ltd., Chuzhou 239000, China*

Bixiao Zhang − *School of Energy and Power, Jiangsu University of Science and Technology, Zhenjiang 212003, China*

Yidan Wei − *School of Energy and Power, Jiangsu University of Science and Technology, Zhenjiang 212003, China*

Complete contact information is available at: https://pubs.acs.org/10.1021/acsomega.4c09980

Author Contributions

Data curation: M.W.and Y.X.; Investigation: M.W., Y.X., M.X., B.Z., and Y.W.; Writing—original draft: M.W., Y.X., and M.X.; Writing—review and editing: M.W., Y.X., B.Z., and Y.W. All authors have read and agreed to the published version of the manuscript.

Notes

The authors declare no competing financial interest.

ACKNOWLEDGMENTS

This work was supported by the National Natural Science Foundation of China (No. 51806089), the General Project of Natural Science Research of Jiangsu Universities (No. 18KJD470001), and the Jiangsu Provincial Graduate Research and Practice Innovation Program (No. KYCX22_3808).

REFERENCES

(1) Chu, S. Carbon Capture and Sequestration. *Science* **2009**, *325* (5948), 1599−1599.

(2) Mattisson, T.; Lyngfelt, A.; Leion, H. Chemical-Looping with Oxygen Uncoupling for Combustion of Solid Fuels. *Int. J. Greenhouse Gas Control.* **2009**, *3* (1), 11−19.

(3) Mattisson, T.; Leion, H.; Lyngfelt, A. Chemical-Looping with Oxygen Uncoupling Using CuO/ZrO2 with Petroleum Coke. *Fuel* **2009**, *88* (4), 683−690.

(4) Zhou, Z.; Han, L.; Nordness, O.; Bollas, G. M. Continuous Regime of Chemical-Looping Combustion (CLC) and Chemical-Looping with Oxygen Uncoupling (CLOU) Reactivity of CuO Oxygen Carriers. *Appl. Catal., B* **2015**, *166*, 132−144.

(5) Ku, Y.; Chang, C. W.; Shiu, S. H.; Wu, H. C.; Moed, N. M. Kinetic Behavior of Fabricated CuO/ZrO_2 Oxygen Carriers for Chemical Looping Oxygen Uncoupling. *Processes* **2021**, *9* (12), 2156.

(6) Skulimowska, A.; Di Felice, L.; Kaminska-Pietrzak, N.; Celinska, A.; Plawecka, M.; Hercog, J.; Krauz, M.; Aranda, A. Chemical Looping with Oxygen Uncoupling (CLOU) and Chemical Looping Combustion (CLC) Using Copper-Enriched Oxygen Carriers Supported on Fly Ash. *Fuel Process. Technol.* **2017**, *168*, 123−130.

(7) Wang, P.; Howard, B.; Means, N.; Shekhawat, D.; Berry, D. Reactivity and Recyclability of Cu-Based Oxygen Carrier in Solid Fuels Chemical Looping with Oxygen Uncoupling (CLOU). *Abstr. Pap. Am. Chem. Soc.*, **2017**, *253*.

(8) Frick, V.; Ryden, M.; Leion, H.; Mattisson, T.; Lyngfelt, A. Screening of Supported and Unsupported Mn-Si Oxygen Carriers for CLOU (Chemical-Looping with Oxygen Uncoupling). *Energy* **2015**, *93*, 544−554.

(9) Shulman, A.; Cleverstam, E.; Mattisson, T.; Lyngfelt, A. Manganese/Iron, Manganese/Nickel, and Manganese/Silicon Oxides Used in Chemical-Looping With Oxygen Uncoupling (CLOU) for Combustion of Methane. *Energy Fuels* **2009**, *23* (10), 5269−5275.

(10) Shulman, A.; Cleverstam, E.; Mattisson, T.; Lyngfelt, A. Chemical-Looping with Oxygen Uncoupling Using Mn/Mg-Based Oxygen Carriers - Oxygen Release and Reactivity with Methane. *Fuel* **2011**, *90* (3), 941−950.

(11) Li, C.; Li, W.; Liao, Y.; Liang, S.; Ma, X. Oxygen Uncoupling Chemical Looping Gasification of Biomass over Heterogeneously Doped La-Fe-O Perovskite-Type Oxygen Carriers. *Fuel Process. Technol.* **2023**, *250*, 107883.

(12) Ryden, M.; Lyngfelt, A.; Mattisson, T. $CaMn_{0.875}Ti_{0.125}O_3$ as Oxygen Carrier for Chemical-Looping Combustion with Oxygen Uncoupling (CLOU)-Experiments in a Continuously Operating Fluidized-Bed Reactor System. *Int. J. Greenh. Gas Control.* **2011**, *5* (2), 356−366.

(13) Abad, A.; Garcia-Labiano, F.; Gayan, P.; de Diego, L. F.; Adanez, J. Redox Kinetics of $CaMg_{0.1}Ti_{0.125}Mn_{0.775}O_{2.9-\delta}$ for Chemical Looping Combustion (CLC) and Chemical Looping with Oxygen Uncoupling (CLOU). *Chem. Eng. J.* **2015**, *269*, 67−81.

(14) Song, H.; Shah, K.; Doroodchi, E.; Wall, T.; Moghtaderi, B. Reactivity of Al_2O_3- or SiO_2-Supported Cu-, Mn-, and Co-Based Oxygen Carriers for Chemical Looping Air Separation. *Energy Fuels* **2014**, *28* (2), 1284−1294.

(15) Samprón, I.; García-Labiano, F.; Izquierdo, M. T.; de Diego, L. F. Understanding the Structural Changes on Fe_2O_3/Al_2O_3 Oxygen Carriers under Chemical Looping Gasification Conditions. *Fuel* **2024**, *355*, 129326.

(16) Liu, G.; Chang, C. C.; Zhao, Y.; Veksha, A.; Giannis, A.; Lim, T. T.; Lisak, G. Effect of Alkali Earth Metal Doping on the CuO/Al_2O_3 Oxygen Carrier Agglomeration Resistance during Chemical Looping Combustion. *J. Cleaner Prod.* **2022**, *366*, 132970.

(17) Narindri Rara Winayu, B.; Shen, B. C.; Chu, H. Impact of Gas Composition (CO, H_2, and HCl) on Chemical Looping Combustion by SiO_2 Supported Oxygen Carriers. *Mater. Chem. Phys.* **2024**, *320*, 129475.

(18) Li, J.; Chen, J.; Zanina, A.; Li, Y.; Yu, C.; Liu, M.; Cui, G.; Wang, Y.; Zhou, M.; Kondratenko, E. V.; Jiang, G. Fundamentals of Enhanced Oxygen Releasability of $Mn\text{-}Na_2WO_4/SiO_2$ through Cofed Water for Efficient Oxidative Coupling of Methane in a Chemical Looping Mode. *J. Catal.* **2023**, *428*, 115176.

(19) Yang, X.; Wu, W.; Ma, S.; Song, T. A Ternary Fe-Based Oxygen Carrier with ZrO_2-$LaFeO_3$ as Support for Chemical Looping Hydrogen Generation. *Int. J. Hydrogen Energy* **2024**, *55*, 756−765.

(20) Abdalla, A.; Tijani, M. M.; Mohamedali, M.; Mahinpey, N. The Effects of WO3 Addition to NiO/ZrO_2 Oxygen Carriers for Chemical Looping Combustion of Methane. *J. Environ. Chem. Eng.* **2022**, *10* (1), 106945.

(21) Narindri Rara Winayu, B.; Li, B.-H.; Chu, H. Fe_2O_3/TiO_2 Oxygen Carrier for Chemical Looping Combustion of CO, H_2, and CH_4 in a Fluidized Bed Reactor. *Mater. Today Commun.* **2022**, *32*, 104026.

(22) Adánez-Rubio, I.; Mattisson, T.; Jacobs, M.; Adánez, J. Development of New Mn-Based Oxygen Carriers Using MgO and SiO_2 as Supports for Chemical Looping with Oxygen Uncoupling (CLOU). *Fuel* **2023**, *337*, 127177.

(23) Ghoniem, A. F.; Zhao, Z.; Uddi, M. Redox Kinetics of NiO/YSZ for Chemical-Looping Combustion and the Effect of Support on Reducibility. *Proc. Combust. Inst.* **2023**, *39* (4), 4477−4487.

(24) Ryu, H. J.; Jin, G. T.; Yi, C.-K. Demonstration of Inherent CO_2 Separation and No NOx Emission in a 50kW Chemical-Looping Combustor : Continuous reduction and oxidation experiment. In *Greenhouse Gas Control Technologies 7*, Rubin, E. S.; Keith, D. W.; Gilboy, C. F.; Wilson, M.; Morris, T.; Gale, J.; Thambimuthu, K., Eds.; Elsevier Science Ltd: Oxford, 2005, pp. 1907−1910.

(25) Adánez, J.; García-Labiano, F.; de Diego, L. F.; Gayán, P.; Abad, A.; Celaya, J. Chapter 34 - Development of Oxygen Carriers for Chemical-Looping Combustion. In *Carbon Dioxide Capture for Storage in Deep Geologic Formations*, Thomas, D. C., Eds.; Elsevier Science: Amsterdam, 2005, pp. 587−604.

(26) Imtiaz, Q.; Kierzkowska, A. M.; Broda, M.; Müller, C. R. Synthesis of Cu-Rich, Al_2O_3-Stabilized Oxygen Carriers Using a Coprecipitation Technique: Redox and Carbon Formation Characteristics. *Environ. Sci. Technol.* **2012**, *46* (6), 3561−3566.

(27) Bao, J.; Li, Z.; Cai, N. Promoting the Reduction Reactivity of Ilmenite by Introducing Foreign Ions in Chemical Looping Combustion. *Ind. Eng. Chem. Res.* **2013**, *52* (18), 6119−6128.

(28) Wang, L.; Shen, L.; Long, Y.; Shen, D.; Niu, X. Intensified Effect of K Adhering to Hematite Involved in the Sulfurous Chemical Looping Gasification. *Fuel* **2023**, *331*, 125767.

(29) Jiang, H.; Huo, R.; Zhang, Z.; Lin, Y.; Zhao, Z.; Hu, J.; Huang, Z.; Huang, H.; Li, H. Dechlorination Performance in Chemical Looping Conversion of Polyvinyl Chloride Plastic Waste Using K/Na/Ca-Modified Iron Ore Oxygen Carriers. *J. Environ. Chem. Eng.* **2022**, *10* (2), 107314.

(30) Liu, T.; Yu, Z.; Jiao, F.; Li, H.; Fang, Y. Effect of Preparation Conditions on the Performance of K-Decorated Fe_2O_3/Al_2O_3 Oxygen Carrier (OC) in Chemical Looping Conversion of Coal Process with Deep OC Reduction. *J. Energy Inst.* **2021**, *98*, 179−187.

(31) Song, G.; Qi, X.; Song, W.; Yang, S.; Lu, Q.; Nowak, W. Slagging Behaviors of High Alkali Zhundong Coal during Circulating Fluidized Bed Gasification. *Fuel* **2016**, *186*, 140−149.

(32) Xiong, R.; Sang, G.; Yan, X.; Zhang, G.; Xu, Q.; Zhang, H. Separation and Characterization of the Active Species in Ti-Doped $NaAlH_4$. *Chem. Commun.* **2013**, *49* (20), 2046−2048.

(33) Iwasaki, C.; Yoshiyama, Y.; Hosokawa, S.; Nagata, N.; Dejima, A.; Onishi, K.; Maeda, R.; Naniwa, S.; Iguchi, S.; Asakura, H.; Teramura, K.; Tanaka, T. Oxygen Storage Property and Catalytic Performance of Ti-Doped $FeNbO_4$. *J. Phys. Chem. C* **2024**, *128* (24), 9884−9893.

(34) Wang, H.; Hou, Y.; Zhang, Y.; Cui, M.; Chen, F.; Huang, X.; Yang, J.; Feng, Z. SO_4^{2-}-Modified La, Y-Doped Ceria-Zirconia with High Oxygen Storage Capacity and Its Application in Pd-Only Three-Way Catalysts. *J. Rare Earths* **2022**, *40* (5), 737−744.

(35) Zhang, L.; Cui, M.; Wang, H.; Hou, Y.; Chen, S.; Zhai, Z.; Long, Z.; Zhang, Y. Effects of Co-Precipitation Temperature on Structure and Properties of La and Y Doped Cerium Zirconium

https://doi.org/10.1021/acsomega.4c09980
ACS Omega 2025, 10, 10308−10316

Mixed Oxides. *Trans. Nonferrous Met. Soc. China* **2022**, *32* (2), 618−628.
(36) Wang, M.; Liu, J.; Hu, J.; Liu, F. O_2−CO_2 Mixed Gas Production Using a Zr-Doped Cu-Based Oxygen Carrier. *Ind. Eng. Chem. Res.* **2015**, *54* (40), 9805−9812.
(37) Ni, C.; Ni, J.; Zhou, Z.; Jin, M. Structural and Chemical Stability of Sr-, Nb- and Zr-Doped Calcium Manganite as Oxygen-Storage Materials. *J. Alloy. Compd.* **2017**, *709*, 789−795.
(38) Kim, K.-J.; Kim, Y. J.; Kim, D. H.; Hong, G.-R.; Lee, Y.-L.; Lee, K.; Roh, H.-S. Zr Doping on CeO_2 Nanocube Catalysts to Enhance Oxygen Storage Capacity for Water-Gas Shift Reaction. *Chem. Eng. J.* **2024**, *495*, 153634.
(39) Galvita, V. V.; Poelman, H.; Bliznuk, V.; Detavernier, C.; Marin, G. B. CeO_2-Modified Fe_2O_3 for CO_2 Utilization via Chemical Looping. *Ind. Eng. Chem. Res.* **2013**, *52* (25), 8416−8426.
(40) Machida, M.; Kawada, T.; Fujii, H.; Hinokuma, S. The Role of CeO_2 as a Gateway for Oxygen Storage over CeO_2-Grafted Fe_2O_3 Composite Materials. *J. Phys. Chem. C* **2015**, *119* (44), 24932−24941.
(41) Maache, R.; Brahmi, R.; Pirault-Roy, L.; Ojala, S.; Bensitel, M. Oxygen Storage Capacity of Pt-CeO_2 and Pt-$Ce_{0.5}Zr_{0.5}O_2$ Catalysts. *Top. Catal.* **2013**, *56* (9−10), 658−661.
(42) Wu, X.; Wu, X.; Liang, Q.; Fan, J.; Weng, D.; Xie, Z.; Wei, S. Structure and Oxygen Storage Capacity of Pr/Nd Doped CeO_2-ZrO_2 Mixed Oxides. *Solid State Sci.* **2007**, *9* (7), 636−643.
(43) Tang, M.; Liu, K.; Roddick, D. M.; Fan, M. Enhanced Lattice Oxygen Reactivity over Fe_2O_3/Al_2O_3 Redox Catalyst for Chemical-Looping Dry (CO_2) Reforming of CH_4: Synergistic La-Ce Effect. *J. Catal.* **2018**, *368*, 38−52.
(44) Zhu, X.; Wei, Y.; Wang, H.; Li, K. Ce−Fe Oxygen Carriers for Chemical-Looping Steam Methane Reforming. *Int. J. Hydrogen Energy* **2013**, *38* (11), 4492−4501.

https://doi.org/10.1021/acsomega.4c09980
ACS Omega 2025, 10, 10308−10316